EUROPEAN TRANSACTIONS ON ELECTRICAL POWER
Euro. Trans. Electr. Power 2011;**21**:1610–1628
Published online 7 December 2010 in Wiley Online Library (wileyonlinelibrary.com). DOI: 10.1002/etep.534

Reliability analysis of voltage instability risk indicator based on a novel real-time identification algorithm

Sandro Corsi[1] and Glauco N. Taranto[2*†]

[1]*CESI Spa., Via Rubattino 54, 20134 Milano, Italy*
[2]*Federal University of Rio de Janeiro, COPPE/UFRJ, 21945-970 Rio de Janeiro, RJ, Brazil*

SUMMARY

This paper focuses the performance and robustness of an algorithm recently proposed in the literature for real-time voltage instability risk indication. Based on local phasor measurements, the real-time identification of the proximity of the equivalent Thevenin impedance seen from an EHV bus and its load impedance is the key to recognize the voltage instability risk at the time it is approaching. The paper highlights the impact of the dynamics of on-load tap changing transformers and generators over-excitation limiters on the Thevenin equivalent identification (and consequently on the timely voltage instability indication). The paper also shows the high reliability of the algorithm with respect to load characteristics and to critical load profiles corresponding to very large perturbations. The paper presents simulation results obtained from a detailed dynamic model of an equivalent single-generator system, as well as from the actual Italian EHV network.

KEY WORDS: voltage stability; PMU; dynamic simulation; long-term voltage stability; Thevenin equivalent; online VSA; voltage stability protection

1. INTRODUCTION

The real-time identification of voltage instability, at the transmission level, significantly contributes to prevent widespread blackouts in practice, as widely recognized around the world. The timely recognition of this risk is crucial to allow effective control and protection interventions at the time they are really needed. Any predictive indicator is useful but with limited help to system protection when compared to a true real-time indicator. The voltage instability analysis at a given bus can be performed by considering the classic Thevenin's equivalent ''seen'' from that bus [1–4], under the assumption of very fast measurements of system electrical variables (use of Phasor Measurement Unit – PMU). The voltage instability is in link with the condition of equality between the absolute value of two equivalent impedances: the load impedance and the Thevenin impedance. Generally speaking, the real-time identification of the Thevenin's equivalent is a difficult problem [1] and the solutions found in the literature [2–4], as proposed, generally require long computing time before convergence. Moreover, they are not supported by a consistent amount of detailed and complete tests to have a clear view and sufficient confidence of their effectiveness on field.

Because of that, the algorithm proposed in Ref. [1] and used in this paper was defined and developed to achieve the objective of a fast and robust real-time identification algorithm. It appears very promising by looking at the results shown in [1,5]. However, before declaring it to be ready for a real system implementation, it is necessary to understand its limitations, and in pursuing that, a comprehensive checking for different operating conditions, critical data and contingencies should be performed. This performance checking is the main contribution of this paper, which shows an

*Correspondence to: Glauco N. Taranto, Federal University of Rio de Janeiro, COPPE/UFRJ, 21945-970 Rio de Janeiro, RJ, Brazil.
†E-mail: tarang@coep.ufrj.br

extensive set of tests that put in evidence the effectiveness of the identification algorithm [1] briefly revisited in this paper.

The tests are performed via time-domain simulation, with the first test being on a single-machine system containing the automatic voltage and frequency controls, on-load tap changing transformer (OLTC), and over-excitation limiter (OEL). These tests are focused on showing the impact OLTCs, OELs, and load characteristics have on the identification of the varying Thevenin parameters, and eventually on the voltage instability risk indication. The tests on a small system also represent reference to better understand results achieved from detailed and large systems. Lastly, they corroborate the results presented in Ref. [6] by showing the relevant differences from one case to another in terms of Thevenin's parameters, and the timing to reach the maximum loadability point (MLP), as well as the ability of the identification algorithm to recognize these differences.

The second set of tests is performed in the actual Italian EHV (380 and 220 kV) network, by considering both load and transit (as defined in Ref. [1]) buses. The tests focus on the effectiveness of the algorithm in a realistic large-scale system including short- and long-term electromechanical dynamic models. Similarly to the small system, the tests highlight the impact of the OLTCs, OELs dynamics, and load pattern variation in the performance of the identification method.

The third set of tests is again performed in the actual Italian EHV network, by considering sharp changes in the slope of load variations, including stepping, and ramping up and down. Since the no-load variation is the worst condition for the algorithm, the minimum acceptable slope is also checked.

The performed analysis reaches the reliability limits of the proposed identification only when imposing too-heavy not-realistic load changes, giving evidence of either the critical aspects impacting on the results, and the robustness of the algorithm in front of real load variations (when including an insensitivity band in front of nearly zero-slope load change).

2. BASICS OF THE PROPOSED IDENTIFICATION ALGORITHM [1]

The circuit shown in Figure 1 represents the entire network "seen" from a load bus in an equivalent form. The maximum power transfer from the equivalent source to the load occurs when:

$$\left|\overline{Z}_{\mathrm{L}}\right| = \left|\overline{Z}_{\mathrm{Th}}\right| \tag{1}$$

with $\overline{Z}_{\mathrm{L}} = Z_{\mathrm{L}}\angle\theta = R_{\mathrm{L}} + jX_{\mathrm{L}}$.

The main purpose of the algorithm proposed in Ref. [1] is the identification of the Thevenin parameters $\vec{E}_{\mathrm{Th}}$ and $\overline{Z}_{\mathrm{Th}}$, based only on the measured phasors $\vec{V}_{\mathrm{L}}$ and $\vec{I}_{\mathrm{L}}$.

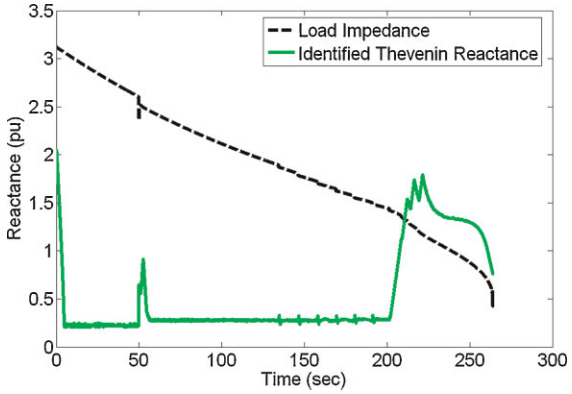

Figure 1. Two-bus Thevenin equivalent circuit.

DOI: 10.1002/etep

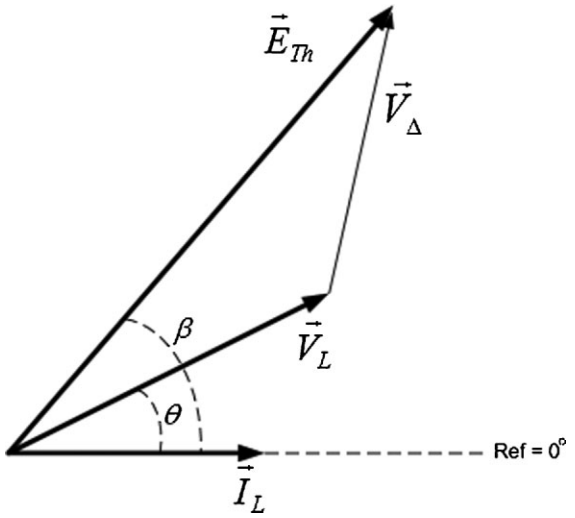

Figure 2. Phasor diagram of the two-bus equivalent circuit.

According to the phasor diagram shown in Figure 2 the following relationship holds:

$$\vec{V}_{\Delta} = \overline{Z}_{\mathrm{Th}} \times \vec{I}_{\mathrm{L}} = R_{\mathrm{Th}} I_{\mathrm{L}} + jX_{\mathrm{Th}} I_{\mathrm{L}} \tag{2}$$

$$\vec{E}_{\mathrm{Th}} = \vec{V}_{\mathrm{L}} + \vec{V}_{\Delta} \tag{3}$$

with $\vec{E}_{\mathrm{Th}} = E_{\mathrm{Th}} \angle \beta$, $\vec{V}_{\mathrm{L}} = V_{\mathrm{L}} \angle \theta$ and $\vec{I}_{\mathrm{L}} = I_{\mathrm{L}} \angle 0°$.

Separating (3) into real and imaginary parts yields:

$$E_{\mathrm{Th}} \cos\beta = R_{\mathrm{Th}} I_{\mathrm{L}} + V_{\mathrm{L}} \cos\theta \tag{4}$$

$$E_{\mathrm{Th}} \sin\beta = X_{\mathrm{Th}} I_{\mathrm{L}} + V_{\mathrm{L}} \sin\theta \tag{5}$$

For the equivalent Thevenin impedance "seen" from an EHV bus, $X_{\mathrm{Th}} \gg R_{\mathrm{Th}}$, and $R_{\mathrm{Th}} \approx 0$ is assumed. Thus,

$$\beta = \cos^{-1}\left(\frac{V_{\mathrm{L}} \cos\theta}{E_{\mathrm{Th}}}\right) \tag{6}$$

Since V_{L} and θ are measured quantities taken from PMUs, the initial estimation of β still depends on E_{Th}. The admissible range for E_{Th} must be in agreement with the electric circuit laws. Up to the MLP and considering an inductive load, its minimum value $\left(E_{\mathrm{Th}}^{\min}\right)$ corresponds to the load voltage, and its maximum value $\left(E_{\mathrm{Th}}^{\max}\right)$ corresponds to the voltage when $Z_{\mathrm{L}} = E_{\mathrm{Th}}$ (with $R_{\mathrm{Th}} = 0$). In normal operating conditions the load impedance is much higher than the equivalent Thevenin impedance. An initial guess for E_{Th} is the arithmetic average of its extreme values (8)

$$E_{\mathrm{Th}}^{0} = \frac{E_{\mathrm{Th}}^{\max} + E_{\mathrm{Th}}^{\min}}{2} \tag{7}$$

where $E_{\mathrm{Th}}^{\min} = V_{\mathrm{L}}$ and $E_{\mathrm{Th}}^{\max} = V_{\mathrm{L}} \cos\theta / \cos\beta$, with β obtained from: $\tan\beta = (Z_{\mathrm{L}} I_{\mathrm{L}} + V_{\mathrm{L}} \sin\theta) / (V_{\mathrm{L}} \cos\theta)$.

Inside the possible range for E_{Th} and X_{Th}, the following facts can be proved [1]: in case of over-estimated E_{Th}, also X_{Th} is over-estimated, and increasing the load impedance (i.e., reducing the power consumption of the load) the value of the estimated E_{Th} also increases. In the case of under-estimated E_{Th}, also X_{Th} is under-estimated, and increasing the load impedance, the value of the estimated X_{Th} decreases. Symmetrical characteristic happens when decreasing the load impedance. So, assuming that E_{Th} and X_{Th} are constant in the brief interval of two consecutive phasor measurements, the proposed adaptive algorithm will reduce E_{Th} when the variation of X_{Th} and the variation of the estimated X_{Th}

DOI: 10.1002/etep

have the same direction, otherwise it will increase E_{Th}. Knowing in which direction E_{Th} should be updated, the size of the variation is parameterized by a constant ε_{E} following the rules developed in Ref. [1].

The adaptive algorithm that tracks the correct value of E_{Th} to identify X_{Th} is repeated here from Ref. [1] for completeness:

2.1. Algorithm to identity X_{Th}

Step 1 – Estimate initial values for E_{Th}^0 according to (7) and β^0 according to (6) already considering E_{Th}^0.
Step 2 – Calculate X_{Th}^0 from (5).
Step 3 – Calculate E_{Th}^i according to the conditions:
If load impedance variation is negative do

$$\mathrm{If}\left(X_{\mathrm{Th}}^{i*}-X_{\mathrm{Th}}^{i-1}\right)<0 \text{ then } E_{\mathrm{Th}}^i=E_{\mathrm{Th}}^{i-1}-\varepsilon_{\mathrm{E}}$$

$$\mathrm{If}\left(X_{\mathrm{Th}}^{i*}-X_{\mathrm{Th}}^{i-1}\right)>0 \text{ then } E_{\mathrm{Th}}^i=E_{\mathrm{Th}}^{i-1}+\varepsilon_{\mathrm{E}}$$

If load impedance variation is positive do

$$\mathrm{If}\left(X_{\mathrm{Th}}^{i*}-X_{\mathrm{Th}}^{i-1}\right)<0 \text{ then } E_{\mathrm{Th}}^i=E_{\mathrm{Th}}^{i-1}+\varepsilon_{\mathrm{E}}$$

$$\mathrm{If}\left(X_{\mathrm{Th}}^{i*}-X_{\mathrm{Th}}^{i-1}\right)>0 \text{ then } E_{\mathrm{Th}}^i=E_{\mathrm{Th}}^{i-1}-\varepsilon_{\mathrm{E}}$$

If load impedance is constant

$$E_{\mathrm{Th}}^i=E_{\mathrm{Th}}^{i-1}$$

Step 4 – Calculate β^i and X_{Th}^i from (6) and (5), respectively.
Step 5 – Increment i and go to Step 3.
OBS: X_{Th}^{i*} is an intermediate evaluation of X_{Th}^{i*} that takes into account the present values of the voltage and current phasor measurements and the previous values of E_{Th} and β.

3. APPLICATION TO A SINGLE-MACHINE SYSTEM

The identification algorithm was tested on an EHV bus (Bus#3) in the system shown in Figure 3. The system consists of a 370MVA synchronous machine, a 20/400 kV step-up transformer, two parallel 400 kV/100 km transmission lines, a 400/132 kV step-down transformer and six parallel 132/20 kV distribution transformers with on-load tap changers (OLTC). The equipment data is realistic and taken from the actual Italian system. The complete network and dynamic data for this system is given in Ref. [6]. The nominal load at Bus#5 is 160 MW (0.43 pu) and 0 Mvar. In all cases defined for this test system, the load increase rate is equal to $\Delta P_{\mathrm{L}}=0.5$ MW/s and $\Delta Q_{\mathrm{L}}=0.5$ Mvar/s according to (8).

$$P_{\mathrm{L}}=(P_{\mathrm{o}}+\Delta P_{\mathrm{L}})\times\left(\frac{V_{\mathrm{L}}}{V_{\mathrm{o}}}\right)^{\alpha},\qquad Q_{\mathrm{L}}=(Q_{\mathrm{o}}+\Delta Q_{\mathrm{L}})\times\left(\frac{V_{\mathrm{L}}}{V_{\mathrm{o}}}\right)^{\beta} \tag{8}$$

where P_{o}, Q_{o}, and V_{o} are nominal values, and α and β are constants to model the load characteristic. For the active and reactive load dependency on voltage the coefficients were set equal to $\alpha=0.7$ and $\beta=2.0$, respectively.

The test consists of ramping up the system load until insurgence of voltage instability characterized by numerical convergence problems in the dynamic simulation program. In addition to the load increase, at 50 seconds, one of the 400 kV transmission lines trips out. One can observe (in Figure 4) a large transient in the identified Thevenin equivalent reactance before reaching, after a few seconds, a new steady-state value. A little before 140 seconds the OLTC starts to actuate and, at approximately 200 seconds, the OEL is reached. The influence of the OLTC in the identification process is not critical. However, the influence of the OEL is of paramount importance as it can be noted in Figure 4. Both

DOI: 10.1002/etep

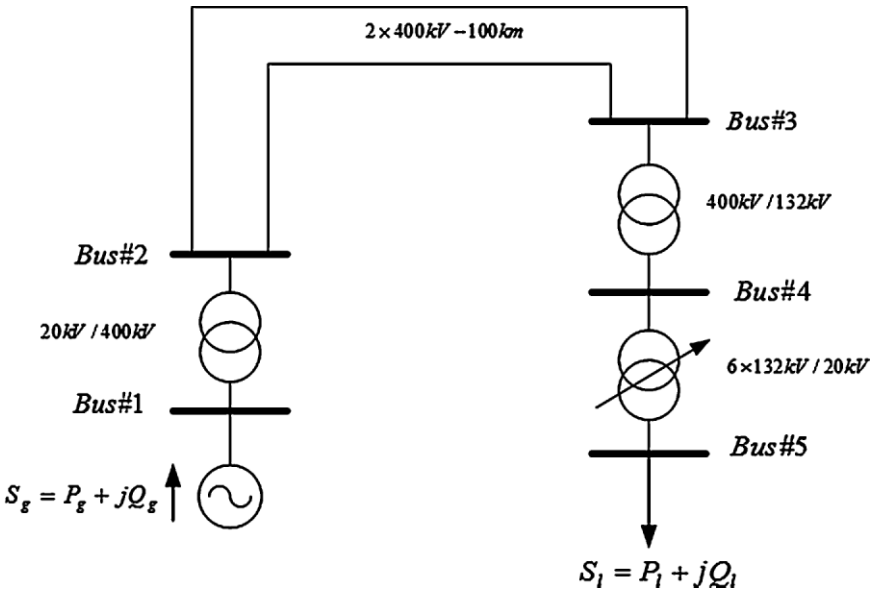

Figure 3. One-line diagram of the single-machine test system.

impedances become equal at the MLP (at 211 seconds), and the simulation runs up to approximately 264 seconds. The period between 211 and 264 seconds is very critical and voltage instability is prone to occur. An additional test consisting of stopping the load increase first at 242 seconds and then at 243 seconds was performed. In the first case the system remains on a stable equilibrium point, whereas in the second case the system loses stability. The test assures the exact point of instability to be at 243 seconds. For practical purposes the indicator gives, in real-time a very good assessment of the voltage instability risk. Figure 5 shows the corresponding identified equivalent Thevenin voltage, together with its corresponding extreme values.

3.1. Performance according to system dynamics

To show the ability of the identification algorithm to distinguish the closed-loop dynamics impact in the system instability, four cases were defined as follows:

Case 1 – OLTC and OEL in service.
Case 2 – OLTC out of service and OEL in service.
Case 3 – OLTC and OEL out of service.
Case 4 – as Case 1 with one transmission line tripped.

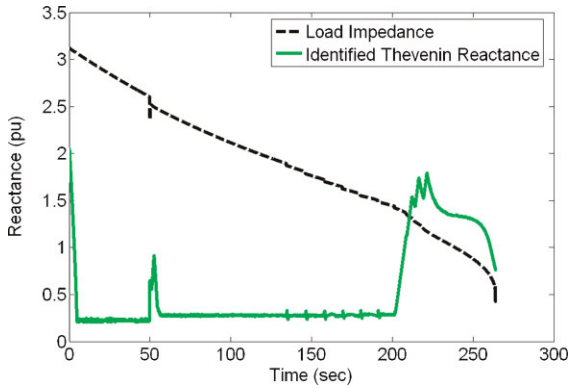

Figure 4. Identification of X_{Th} as system load ramps up.

DOI: 10.1002/etep

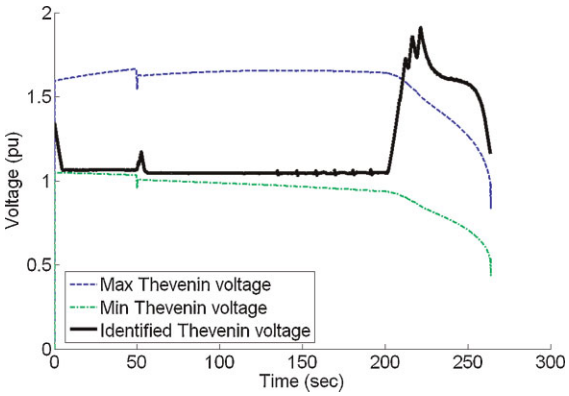

Figure 5. Identification of E_{Th} as system load ramps up.

Figure 6 shows the identified X_{Th} for the four cases previously described. The following comments can be drawn from Figure 6:

Early voltage instability risk identification is inferred for Case 4 (dotted line). The closed-loop controls (OLTC and OEL) and the transmission line tripping are responsible for the voltage collapse anticipation.
Inevitably large transients occur in the identified X_{Th} in front of a system contingence (like line tripping). The fast recovery shows this could be a limitation of the proposed method only in proximity of voltage instability, as transient anticipation of the incoming event. Utilizing a moving average of X_{Th}, consequently slowing down the identification process, can mitigate this transient. The cases in Figures 4–6 do not use the moving average.
The correct increase of X_{Th} after the line tripping.
A sharp increase in X_{Th} when the OEL starts to operate in Cases 1, 2, and 4 (dash-dotted, dashed, and dotted lines, respectively).
An anticipation of voltage instability by the OLTC actuation (comparison between Cases 1 and 2), and its small influence on X_{Th}.
The correct invariability of X_{Th} in Case 3.

Overall, due to the real-time computing ability of the tested algorithm, each point of the represented plots is computed at the correspondent instant in the time scale, i.e., there is no delay between the system evolution and the corresponding algorithm output. Moreover, the proposed algorithm adequately identified the equivalent Thevenin parameters, showing the relevant differences, in terms of time and load values, for each of the considered working conditions, as confirmed by the tests to be shown in the following Subsection 3.2.

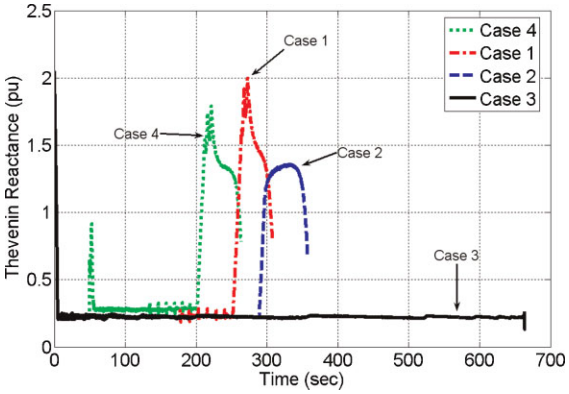

Figure 6. Identification of X_{Th} for distinct consideration of close-loop controls.

DOI: 10.1002/etep

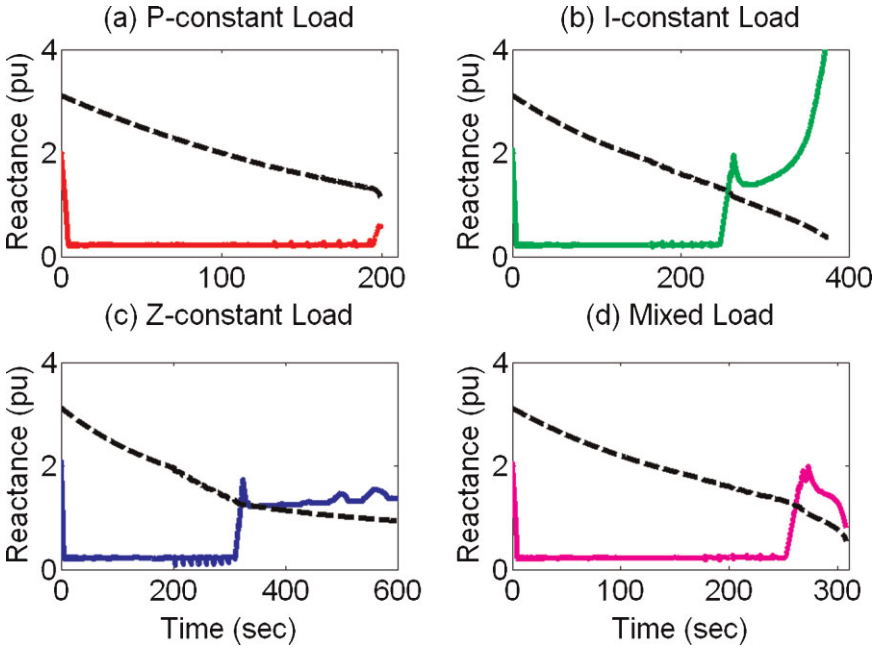

Figure 7. Identification of X_{Th} as a function of the load type.

3.2. *Performance according to load characteristic*

The performance of the E_{Th} identification method was also tested for different load types, as shown in Figure 7. The dashed line corresponds to the load impedance. The system was set in Case 1 and the load modeled as a static 100% *P*-constant (subplot (a)), 100% *I*-constant (subplot (b)), 100% *Z*-constant (subplot (c)), and mixed with $\alpha = 0.7$, $\beta = 2.0$ (subplot (d)).

The intersection (MLP) between the load and the X_{Th} identification curves occurs at different instants: before 200 seconds for the *P*-constant and at 262, 257, and 317 seconds for mixed, *I*-constant, and *Z*-constant load type, respectively. It can be noted the ability of the method to distinguish the different MLPs mainly driven by the OEL action. For the mixed-type (the more realistic) and the *I*-constant loads, the voltage collapse occurs 46 and 119 seconds after MLP, respectively. Again, this is the time characterized by numerical convergence problems in the dynamic simulation program. Reference [6] shows that, during the time period between the MLP and the voltage collapse points, the system is prone to voltage instability. Normally, in such period the system voltages sag sharply and progressively while protective apparatuses start operating, as it can be seen in Figure 8 for the *I*-constant load characteristic simulation. At 257 seconds (at MLP) the voltage at Bus#3 is 0.93 pu and the voltage at Bus#5 is 0.88 pu, whereas at 376 seconds (simulation end) the voltage at Bus#3 is 0.34 pu and the voltage at Bus#5 is 0.02 pu.

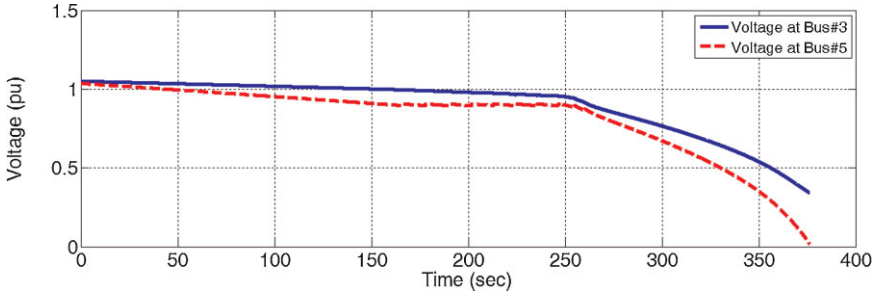

Figure 8. Voltages at Bus#3 and Bus#5 for the *I*-constant load characteristic.

DOI: 10.1002/etep

4. APPLICATION TO THE ITALIAN 380–220 KV NETWORK

The Italian system analyzed contains the actual 380 and 220 kV networks. The system configuration has 2549 buses, 2258 transmission lines, 134 groups of thermal generators, and 191 groups of hydro generators. Short- and long-term dynamic models are utilized in the time-domain simulations. The system load is approximately 50 GW, represented as a static model with $\alpha = 0.7$ and $\beta = 2.0$ in (13). The system is under primary voltage and frequency controls only.

The voltage and current phasors are measured with a sampling rate of 20 ms. The Thevenin parameter identification is updated every 20 ms, while the identified value is based on the sampled data of the last 80 ms.

The tests on the Italian system were performed at the Poggio a Caiano 380 kV load bus located at Firenze area depicted in Figure 9, and at the Baggio 380 kV transit bus located at Milano Area. The analysis performed in the Firenze area consisted of increasing the local area load by a rate of 10%/minute maintaining constant the power factor. The load at Poggio a Caiano 380 kV and Casellina 220 kV buses were increased by a rate of 40%/minute. The objective of such load increase profile is to ensure the buses prone to voltage instability, and not to find which bus in the system will first face voltage instability. Obviously, the algorithm could also be used for the latter objective, analogously to the works reported in Ref. [2–4]. The load increase at Milano area for the tests at Baggio bus followed the same profile described in Ref. [1].

The analyses performed in Poggio a Caiano, like it was done in the single-machine system, are twofold – to show the impact of the system dynamics, and the load characteristic in the performance of the identification algorithm. Whereas, the analyses at Baggio bus shows only the impact of the system dynamics on the algorithm results.

4.1. Poggio a Caiano load bus

4.1.1. Performance according to system dynamics. To show the ability of the algorithm to identify the impact of different closed-loop dynamics in the stability performance in the Italian system, four cases were defined as follows:

Case 1 – all OELs in service and only Poggio a Caiano OLTCs in service.
Case 2 – all OELs in service and all OLTCs out of service.
Case 3 – all OELs and OLTCs out of service.
Case 4 – all OELs and OLTCs in service.

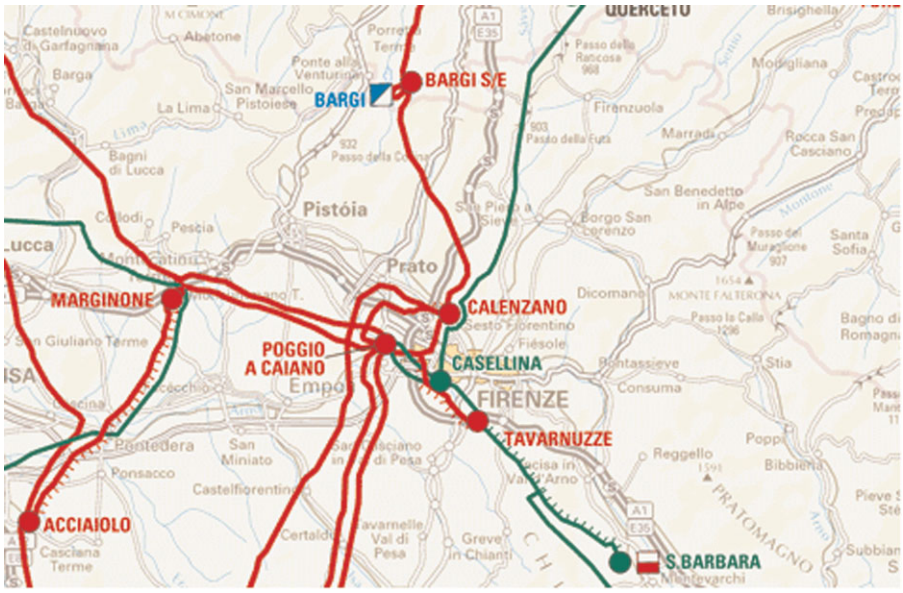

Figure 9. Detail of the Firenze area showing the Poggio a Caiano 380 kV bus.

DOI: 10.1002/etep

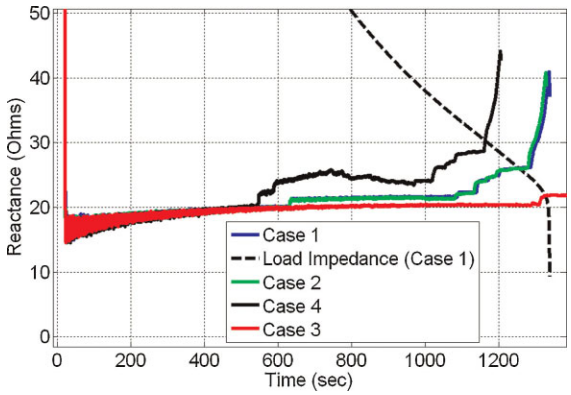

Figure 10. Identification of X_{Th} for distinct consideration of close-loop controls.

Cases 2 and 4 represent more realistic situations, and Cases 1 and 3, even though being less realistic are worth showing for comparison purposes. Figure 10 shows the identified Thevenin reactance for all cases. It also shows the impedance load (dashed line) for Case 1 only. As one would expect, Case 4 is the one where voltage instability occurs earlier, being well pointed out by the identification algorithm. The slight difference between Cases 1 and 2 is also well captured by the algorithm. In Case 3, X_{Th} maintains fairly constant since the OELs and OLTCs are out of service.

Figure 11 shows the voltage at Poggio a Caiano 380 kV bus in the four cases. It is worth nothing that in the tests performed at Poggio a Caiano Bus the MLP was reached at a voltage profile lower than 0.85 pu (340 kV for a base voltage of 400 kV). In fact in this case, differently from the most common voltage instability approaching, under voltage protection would actuate before the MLP. Nevertheless, this result does not invalidate the purpose of the identification algorithm. In a practical implementation one would utilize the voltage instability index in conjunction with and not in replacement of others protective apparatuses.

To further investigate the analysis done for Poggio a Caiano bus, we detail the results of two cases. Figures 12–14 show simulating results for Case 1, and Figures 15–17 show simulating results for Case 4.

Figure 12 shows the identified X_{Th} and Figure 13 shows the evolution of the OEL indicator of six groups of generators electrically close to Poggio a Caiano bus. When this indicator reaches zero, the machine OEL begins to work in closed loop. The OEL model is of the summing type with soft limiting, which retains the normal voltage regulator loop [7]. Figure 14 shows the tap position of the two OLTCs at Casellina bus. It can be noted that a continuous tap variation model was employed in the SICRE simulator [8]. The OLTCs cease to operate when their tap position reaches 0.8 (lower tap limit).

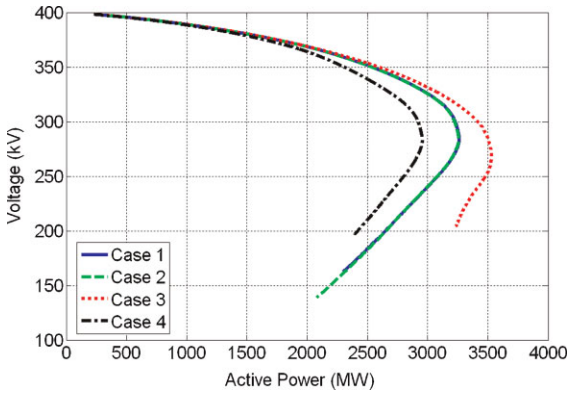

Figure 11. Voltage at Poggio a Caiano 380 kV bus.

DOI: 10.1002/etep

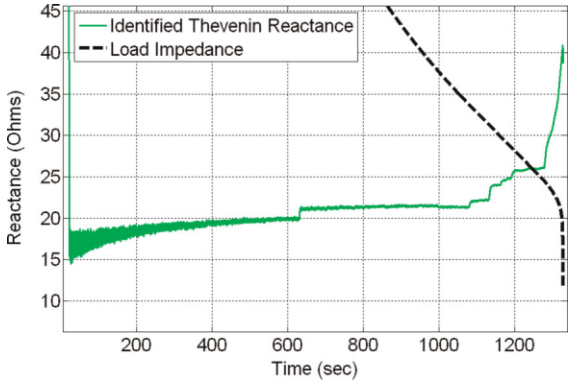

Figure 12. Identification of X_{Th} in Case 1.

Comparing the figures, one can note that when La Spezia OEL starts to operate (around 600 seconds) the identified Thevenin impedance visibly has its value increased. This is explained by the fact that when the generator reaches its over-excitation limit the synchronous reactance now becomes part (and a big one) of the equivalent Thevenin impedance. The figures also show the fast variation of the Thevenin impedance (from 1100 to 1200 seconds) when the system is approaching its MLP, with the OLTCs ceasing to operate and the remaining nearby OELs starting to operate.

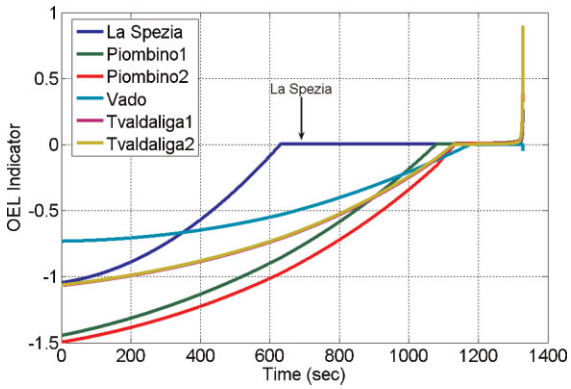

Figure 13. OEL indicator of six electrically close group of generators in Case 1.

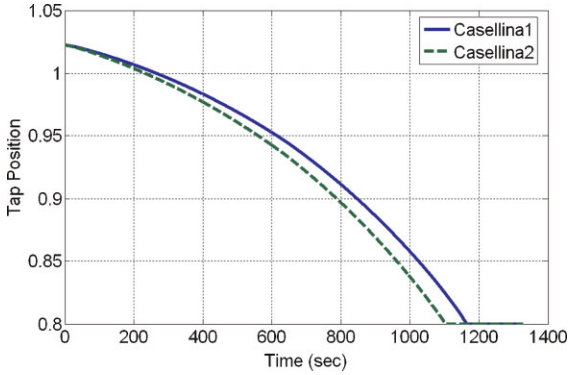

Figure 14. Tap position of the two Casellina OLTCs in Case 1.

DOI: 10.1002/etep

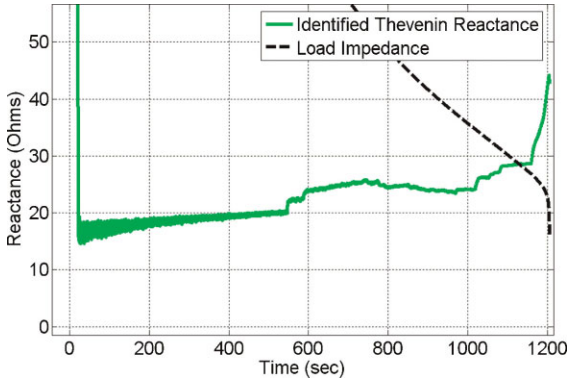

Figure 15. Identification of X_{Th} in Case 4.

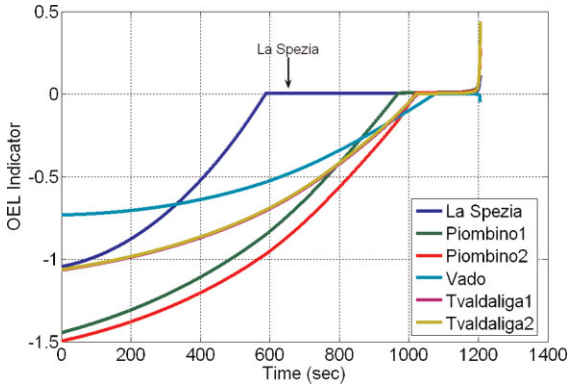

Figure 16. OEL indicator of six electrically close group of generators in Case 4.

Similar conclusions can be drawn from the results obtained for Case 4. Figures 15–17 shows the identified X_{Th}, the OEL indicator of the same six electrically close group of generators, and the tap position of some OLTCs, respectively.

4.1.2. Performance according to load characteristic. Analogously to the analysis performed to the single-machine system, the performance of the proposed method was also tested in the Italian system for different load types. The system was set in Case 4 and the loads modeled as a static

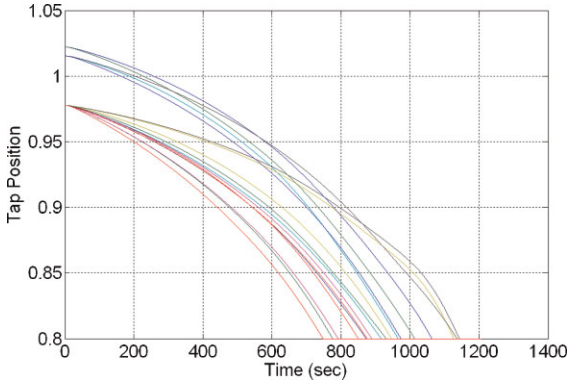

Figure 17. Tap position of some OLTCs in Case 4.

DOI: 10.1002/etep

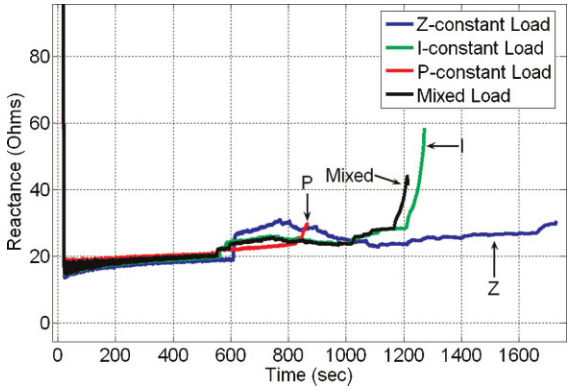

Figure 18. Identified Thevenin reactance as a function of the load type.

100% *P*-constant, 100% *I*-constant, 100% *Z*-constant, and mixed (original load type with $\alpha = 0.7$, $\beta = 2.0$).

Figures 18 and 19 show the identified E_{Th} for the various load types and the simplest voltage instability risk indicator defined as the ratio of the identified Thevenin reactance (X_{Th}) and the load impedance (Z_{L}). In all cases, it is important to note the slope change of the indicator when the voltage instability is approaching. All the results match those given in Session II.

4.2. Baggio transit bus

As mentioned before, for the Baggio 380 kV transit bus (according to the definition given in Ref. [1]) we show the performance of the algorithm only as distinct results affected by different OLTC and OEL combinations.

Three cases were defined as follows:

Case 1 – OELs and OLTCs in service.
Case 2 – OELs in service and OLTCs out of service.
Case 3 – OELs and OLTCs out of service.

Figure 20 shows the identified Thevenin reactance for all cases and the impedance load (dashed line) for Case 3 only. The results qualitatively confirms those obtained in the load buses like Poggio a Caiano and Bus#3 in Figure 3, including the maintainability of X_{Th} fairly constant up to MLP in case OELs and OLTCs are out of service. However, the point to highlight is the ability of the algorithm to clearly distinguish the differences with or without the control systems, also when considering a transit

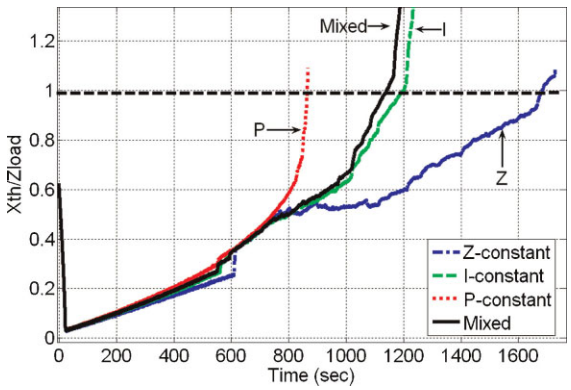

Figure 19. Voltage instability indicator as a function of the load type.

DOI: 10.1002/etep

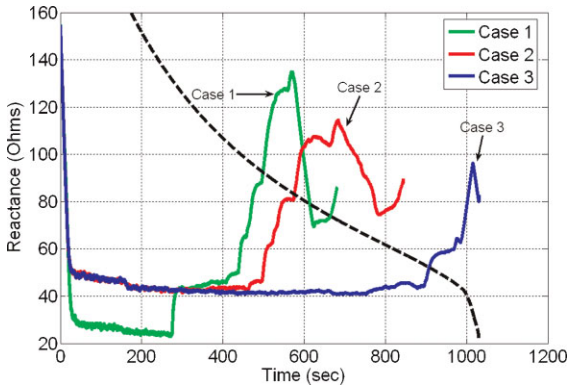

Figure 20. Identification of X_{Th} for distinct consideration of close-loop controls.

bus. The difference of X_{Th} in the first seconds, as seen in Case 1, is mainly due to the OLTCs operation. Figure 21 shows the voltage instability risk indicator corresponding to the three cases defined for the Baggio bus.

5. APPLICATION WITH CRITICAL LOAD VARIATION PROFILE

This section exploits the strength and weakness of the proposed algorithm when the system faces critical load variation profiles. The results presented in this section were obtained either from tests with the Italian network at the Poggio a Caiano bus or from tests with the single-machine system at Bus#3.

5.1. Saw-toothed load variation

This subsection shows the performance of the identification algorithm when the system faces a saw-toothed variation superimposed to an increase load ramp, as depicted in Figure 22. Figure 23 is a zoomed image of the curves shown in Figure 22. It can be noted that at the points the load curve slope changes, there is a transient in the identification of X_{Th}. However, the identification method is able to fast recover the correct value of X_{Th}. Figure 24 shows the voltage instability risk indicator, it refers to a situation where the indicator nearly reaches the unit value at about 900 seconds, and reduces afterwards. In this case the test shows that a false alarm could happen. The algorithm performance was very satisfactory in such situation, giving also evidence of the relevant impact of the load slope changes on the identification transients, as well as of their fast recovery.

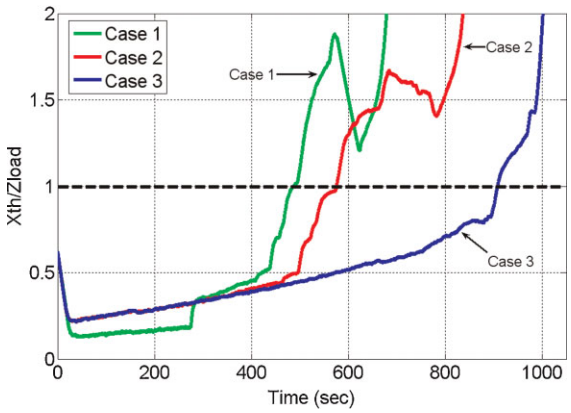

Figure 21. Voltage instability indicator for distinct considerations of close-loop controls.

DOI: 10.1002/etep

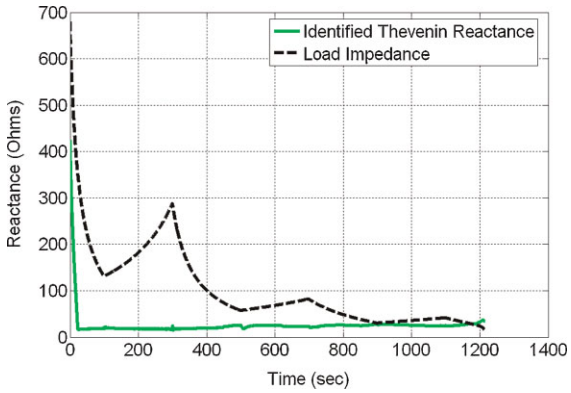

Figure 22. Saw-toothed load.

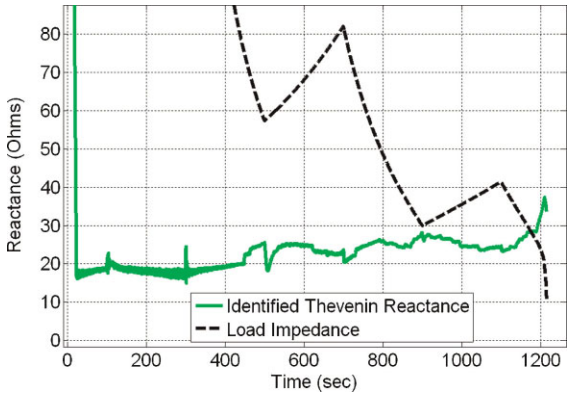

Figure 23. Identification of X_{Th} for a saw-toothed load variation.

5.2. *Minimum slope variation*

In order to show the critical impact of the minimum load variation, the identification algorithm was tested with load ramping at different slopes. All the tests start with a ramp of high slope to allow the algorithm to quickly initialize to the correct X_{Th} value, and then change to a lower slope ramp. The tests are performed in the most critical operating conditions for the algorithm, i.e., far away from the MLP.

Figure 25 shows X_{Th} as a function of the rate of change of the load, from the tests with the single-machine system at Bus#3. The initial load for this test was set equal to $P_{\mathrm{l}} = 100$ MW and $Q_{\mathrm{l}} = 10$ Mvar.

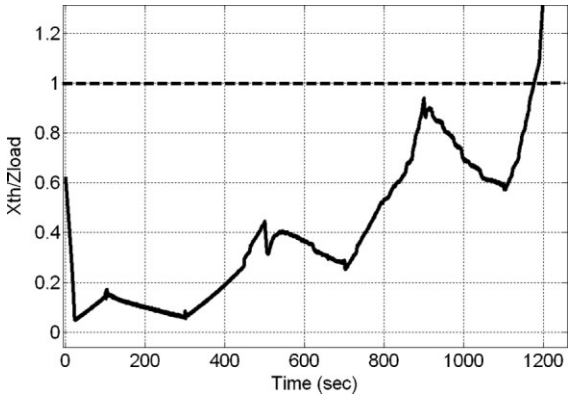

Figure 24. Voltage instability indicator for a saw-toothed load variation.

DOI: 10.1002/etep

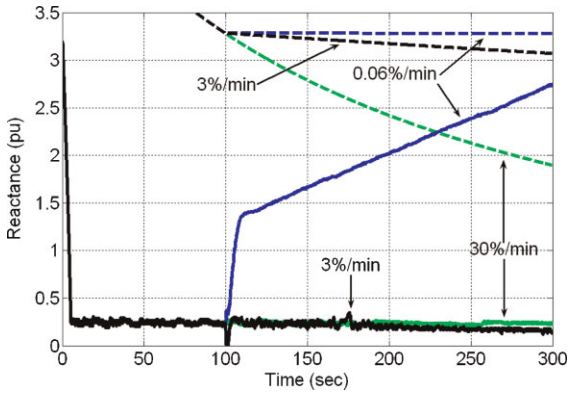

Figure 25. X_{Th} identification as a function of the load rate of change. Dashed lines correspond to the load impedances.

A rate of change of 30%/minute (30 MVA/min) is applied up to 100 seconds. From 100 to 300 seconds, the figure shows the cases for 30, 3, and 0.06%/minute. Figure 25 also shows (in dashed line) the corresponding load impedances for the three cases. It can be noted that with a rate of change of 0.06%/minute, corresponding to 20 VA every 20 ms, the proposed algorithm diverges from the correct value of X_{Th}.

Figure 26 shows the identification of X_{Th} as a function of the load rate of change at Poggio a Caiano. From 0 to 200 seconds the load rate of change is 40%/minute (76 MW/min) in both curves. From 200 to 600 seconds Curve 1 and Curve 2 correspond to a change of 20 and 0.5%/minute, respectively. The algorithm is capable to correctly identify X_{Th} when the load ramp changes from 40 to 20%/minute. However, it starts to have difficulties when the rate of change is 0.5%/minute (i.e., 380 VA in 20 ms).

From the tests performed in both systems, we can conclude that the algorithm was able to adequately and robustly identify the correct value of X_{Th} for the real load slope variations (higher than few kW/second). With lower load variations there is a need to ''freeze'' the algorithm. Inside this dead band the value of X_{Th} does not change with respect to the previous correct one.

5.3. *Step load variation*

The identification algorithm has also been tested when the system faces load step variations. To explore the performance in front of steps by themselves, the load is changed after the steps with a high slope values. The cases with 20 and 2%/minute slopes are analyzed at the Poggio a Caiano bus. Figure 27

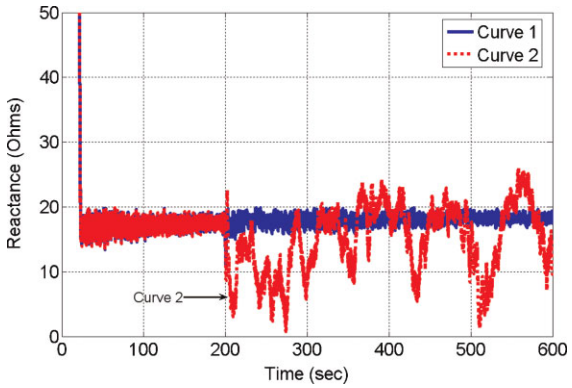

Figure 26. X_{Th} identification as a function of the load rate of change.

DOI: 10.1002/etep

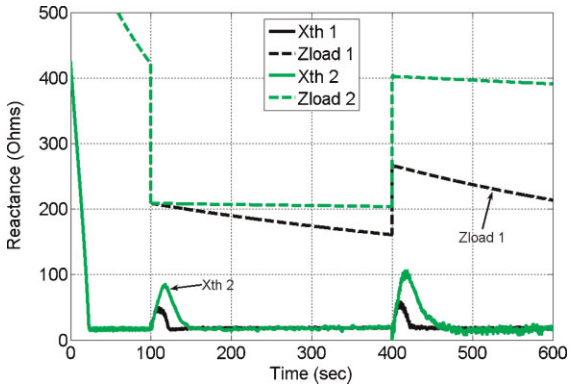

Figure 27. X_{Th} identification as affected by load step changes. Dashed lines correspond to the load impedances.

shows X_{Th} as affected by load step changes. The algorithm initialization lasts the first 100 seconds. At 100 seconds occurs a positive step variation of 100% of the initial load followed at 400 seconds by a negative step of 100%. From 100 to 600 seconds the cases with the slope equal to 20 and 2%/minute are shown. The performance of the algorithm is adequate in front of the large step changes in the load. The X_{Th} identification traces die out in about 25 and 50 seconds for the cases with slope of 20 and 2%/minute respectively, confirming the identification robustness.

5.4. *Step and ramp load variation*

In this subsection we show a very difficult condition to the algorithm where we combine high frequency load stepping (50 seconds-duration pulses) and ramps with small slope.

5.4.1. Step sequence with 20% slope in the flat part. Figures 28 and 29 show the identification of the equivalent Thevenin voltage and reactance, respectively, for a load variation consisting of steps having a 20% slope in its flat part. The performance of the algorithm is acceptable for this case.

Figure 30 shows a zoomed plot of the curves in Figure 29. Note that a slow transient starts at the points where the step change occurs, but before settling to the correct value for X_{Th}, the subsequent step variation occurs and the algorithm continues the hunting for a new value for X_{Th}. Figure 31 highlights these transients in the voltage instability risk indicator.

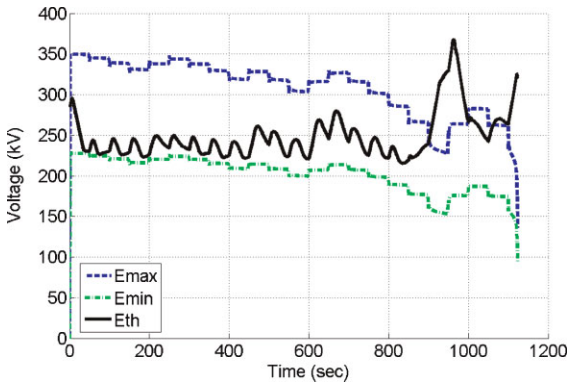

Figure 28. Identification of E_{Th} for load steps having a 20% slope in its flat part.

DOI: 10.1002/etep

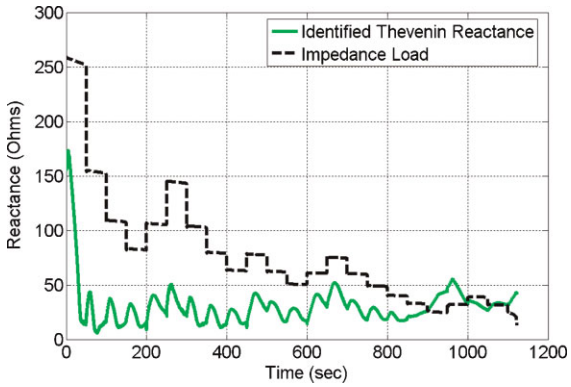

Figure 29. Identification of X_{Th} for load steps having 20% slope in its flat part.

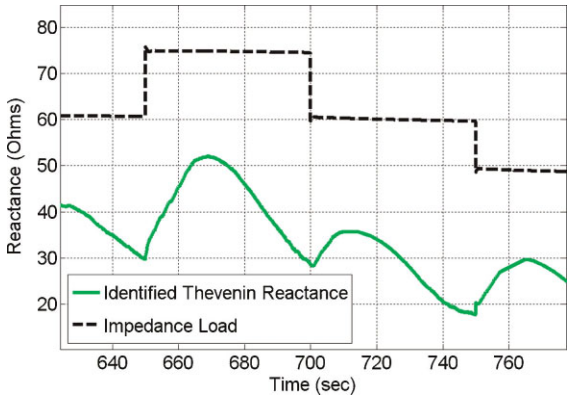

Figure 30. Zoomed image of the curves presented in Figure 29.

5.4.2. Step sequence with 2% slope in the flat part. Figures 32 and 33 show the identification of the equivalent Thevenin voltage reactance, for a load variation consisting of steps having a 2% slope in its flat part. The algorithm fails to identify the Thevenin parameters. The case by imposing $E_{\mathrm{Th}}^{\min} \leq E_{\mathrm{Th}}^{\max}$ also fails. This test was performed to enforce the algorithm to its limit of validation, combining minimum slope with very large unusual perturbations. Therefore, this is an important test for assessing

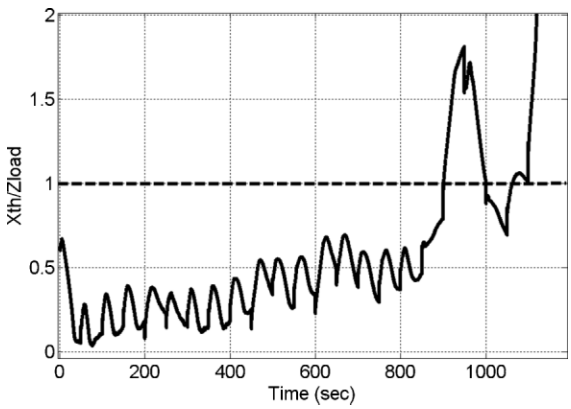

Figure 31. Voltage instability indicator for load steps having 20% slope in its flat part.

DOI: 10.1002/etep

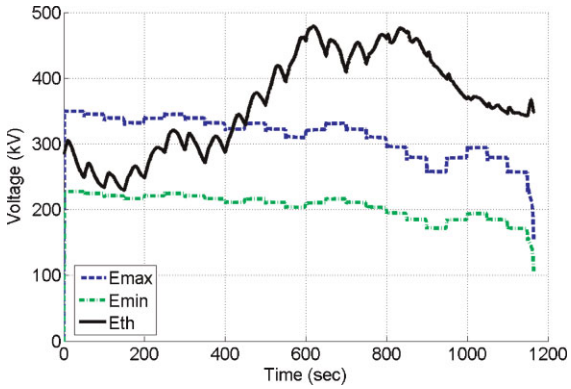

Figure 32. Identification of E_{Th} for load steps having a 2% slope in its flat part.

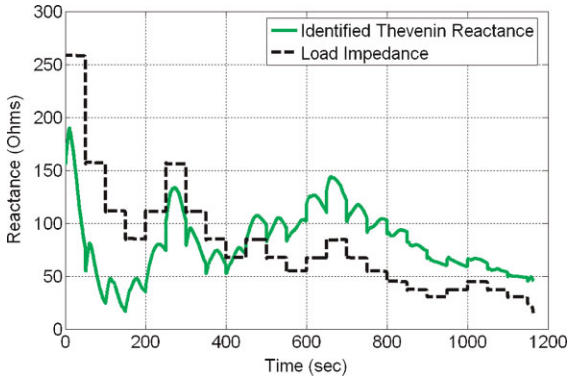

Figure 33. Identification of X_{Th} for load steps having a 2% slope in its flat part.

the algorithm robustness. This is also a confirmation that the algorithm has to be protected against the minimum slope load variation, as already shown before by the test shown in Subsection B.

6. CONCLUSIONS

The comprehensive tests on the innovating real-time voltage instability detection algorithm, gives wide evidence of its effectiveness and robustness in front of real power system operating conditions, as well as of its ability to work well also in front of not-real too-heavy working conditions. The only recognized limit is due to the case of no load variation, but in that case, there is no need to update the last estimated values.

The algorithm recognizes in a very fast way the rising of the voltage instability phenomenon seen by an EHV bus provided with PMU, notwithstanding the intrinsic difficulties to identify, in real time, the Thevenin's equivalent circuit seen by the considered EHV bus. The algorithm has been deeply tested through a comprehensive dynamic analysis, in front of normal and unusual load variation, also considering different load characteristics. The effectiveness of the algorithm resulting from the tests on the single machine equivalent system, has been also confirmed by the dynamic tests performed on the Italian large power system represented by a detailed simulation model, both on load and on transit buses. All the results are meaningful, in agreement with those presented in [1,5,6]. Moreover, according to the results given in Ref. [5], any possible voltage stability indicator based on the analyzed identification algorithm, provides real-time performance and high reliability. The need to endow the algorithm with a dead band in front of nearly zero-slope load change is confirmed.

DOI: 10.1002/etep

7. LIST OF ABBREVIATIONS

EHV	Extra high voltage
MLP	Maximum loadability point
OEL	Over-excitation limiter
OLTC	On-load tap changer
PMU	Phasor measurement unit

ACKNOWLEDGEMENTS

The authors would like to acknowledge Ferdinando Parma, Massimo Salvetti, and Massimo Pozzi for their contributions regarding the SICRE simulator, and Giuseppe Cappai and Ivan Valade for their contributions regarding the DigSilent simulator. G. N. Taranto acknowledges the financial support provided by CNPq and CESI on his sabbatical year.

REFERENCES

1. Corsi S, Taranto GN. ''A Real-time voltage instability identification algorithm based on local phasor measurements''. *IEEE Transactions on Power Systems* 2008; **23**(3): 1271–1279.
2. Vu K, Begovic MM, Novosel D, Saha MM. ''Use of local measurements to estimate voltage-stability margin''. *IEEE Transactions on Power Systems* 1999; **14**(3): 1029–1035.
3. Milosevic B, Begovic M. ''Voltage-stability protection and control using a wide-area network of phasor measurements''. *IEEE Transactions on Power Systems* 2003; **18**(1): 121–127.
4. Smon I, Verbic G, Gubina F. ''Local voltage-stability index using Tellegen's theorem''. *IEEE Transactions on Power Systems 2006;* **21**(3): 1267–1275.
5. Corsi S, Taranto GN, Guerra LNA. ''A New real-time Voltage Stability Indicators Based on Phasor Measurement Unit Data'', Paper C4-109, CIGRÉ Session, Paris, August 2008.
6. Corsi S, Taranto GN. ''Voltage Stability – the Different Shapes of the ''Nose'', Proceedings of the Bulk Power Systems Dynamics and Control VII, IREP Conference, Charleston, SC, August 2007.
7. IEEE Task Force on Excitation Limiters. ''Recommended models for overexcitation limiting devices''. *IEEE Transactions on Energy Conversion* 1995; **10**(4): 706–713.
8. Scarpellini P. Cova B, Marconato R, *et al.* ''A Powerful Simulator for Investigating Severe Dynamic Phenomena During System Major Distarbance''. Paper 38-305, CIGRÉ Session, Paris, August 1996.

DOI: 10.1002/etep